
Article:
Quintana-Gomez, L., Connolly, M., Shehab, A. et al. (2 more authors) (2022) "Reverse combustion" of carbon dioxide in water: the influence of reaction conditions. Frontiers in Energy Research, 10. 917943. ISSN 2296-598X

https://doi.org/10.3389/fenrg.2022.917943

---

frontiers | Frontiers in Energy Research

TYPE Original Research
PUBLISHED 19 August 2022
DOI 10.3389/fenrg.2022.917943

OPEN ACCESS

EDITED BY
Obid Tursunov,
Tashkent Institute of Irrigation and Melioration, Uzbekistan

REVIEWED BY
Bruna Rego de Vasconcelos,
Université de Sherbrooke, Canada
Alexandr Kustov,
National University of Science and Technology MISiS, Russia

*CORRESPONDENCE
James McGregor,
james.mcgregor@sheffield.ac.uk

†PRESENT ADDRESS
Ali Al-Shathr,
Chemical Engineering Department,
University of Technology-Iraq,
Baghdad, Iraq

SPECIALTY SECTION
This article was submitted to Carbon Capture, Utilization and Storage, a section of the journal Frontiers in Energy Research

RECEIVED 11 April 2022
ACCEPTED 19 July 2022
PUBLISHED 19 August 2022

CITATION
Quintana-Gómez L, Connolly M, Shehab AK, Al-Shathr A and McGregor J (2022), "Reverse combustion" of carbon dioxide in water: The influence of reaction conditions.
Front. Energy Res. 10:917943.
doi: 10.3389/fenrg.2022.917943

"Reverse combustion" of carbon dioxide in water: The influence of reaction conditions

Laura Quintana-Gómez[1,2], Matthew Connolly[1], Amal K. Shehab[1], Ali Al-Shathr[1†] and James McGregor[1*]

[1]Department of Chemical and Biological Engineering, University of Sheffield, Sheffield, United Kingdom, [2]Department of Chemical Engineering and Environmental Technology, BioEcoUva, Research Institute on Bioeconomy, High Pressure Process Group, Universidad de Valladolid, Valladolid, Spain

The synthesis of value-added organic products from the hydrothermal conversion of CO_2 and H_2O has been demonstrated, revealing the impact that reaction conditions have on the product distribution and yield. CO_2 has the potential to become a valuable feedstock for the chemicals sector, in part displacing fossil resources and improving the economics of carbon capture. Herein the conversion of CO_2 with H_2O, in the absence of gas-phase H_2, to methanol and other products is shown to occur under sub-critical water conditions in the presence of iron as a reductant and catalyst: this process can be considered as a form of "reverse combustion". The influence of reaction temperature between 200–350°C and CO_2:O_2 mole ratio from 9 to 119 (in addition to pure 100% CO_2) have been investigated in the presence of Fe powder. The influence of reaction time has also been investigated, employing Fe_3O_4 as a catalyst. Product analysis is conducted by GC-MS and MS for liquid- and gas-phase products respectively, while SEM and XRD are employed to analyse morphological changes in the catalyst and TPO investigates any coke deposited during reaction. Methanol is the major product formed at all conditions investigated, with a maximum concentration of 8 mmol L^{-1} after 12 h of reaction, or after 4 h in the presence of oxygen. Acetone and ethanol are also formed, although in smaller quantities than methanol, with larger-chained species also present. An inverse relationship is observed between acetone and ethanol concentrations. Based on the analysis of the reaction data it is hypothesized that ethanol and acetone may be competitively produced in one reaction pathway, while methanol is produced in an independent, parallel, pathway. The observation of acetaldehyde in the gas-phase at all studied conditions suggests that acetone may be produced from the dehydrogenation of ethanol via an acetaldehyde intermediate; catalyzed by zero-valent iron sites. Morphological characterization indicates that the catalysts are stable under the reaction conditions. These studies facilitate the development of improved catalysts and processes for the hydrothermal conversion of CO_2, allowing further development of this promising sustainable process.

KEYWORDS

carbon dioxide utilization, high temperature water, methanol synthesis, iron catalysis, circular economy

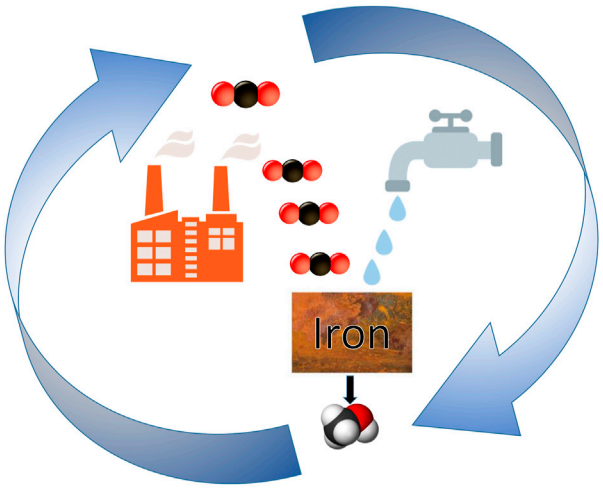

Graphical Abstract

Introduction

The combustion of fossil fuels along with deforestation has broken the natural balance of the Earth´s carbon cycle. As a consequence, CO_2 concentration in the atmosphere has increased from approximately 278 ppm in ca. 1750 (Stocker et al., 2013) to 418.8 ppm in March 2022 (Global Monitoring Laboratory, 2021), playing a leading role in the changes to the global climate (Mac Dowell et al., 2017). To reduce CO_2 emissions, CO_2 can be captured directly from air (Keith et al., 2018) or from power and chemical plants (De Guido et al., 2018) using amine solvents, ionic liquids, solid sorbents, advanced membranes and porous materials (Omodolor et al., 2020). This abundant and low cost CO_2 can become a feedstock for the chemical industry by acting as a C_1 building block to produce value-added chemicals and fuels which are presently obtained predominately from fossil sources (Zhong et al., 2019a). Moreover, the use of captured CO_2 to produce value-added products may partially compensate for the high costs associated with carbon capture and storage (CCS), thereby improving the economic feasibility of such schemes (Styring et al., 2011).

Many methods such as catalytic hydrogenation, or electrochemical or photochemical reactions have been proposed for the direct conversion of CO_2. However, photochemical and electrochemical reduction of CO_2 present a low efficiency, thereby limiting their application (Zhu et al., 2019). Although catalytic hydrogenation of CO_2 has arisen as a promising and feasible technique for CO_2 utilisation, it typically requires the addition of gas-phase hydrogen (Zhong et al., 2019a). Commercial hydrogen is at present mainly produced by steam reforming of methane (SMR), which produces CO_2 as a by-product, and is highly energy intensive due to the endothermic nature of the reaction (Michalkiewicz and Koren, 2015). While much effort is devoted to exploring more sustainable routes to H_2 generation, these remain economically uncompetitive with SMR at present (Jovan and Dolanc, 2020). Moreover, hydrogen utilisation involves transportation, storage and safety concerns (Zhu et al., 2019).

As an alternative to the use of gaseous H_2, high temperature water (HTW) can be regarded as a potential hydrogen donor and reaction medium. HTW presents a lower dielectric constant, fewer and weaker hydrogen bonds and higher isothermal compressibility in comparison to water at room temperature (Akiya and Savage, 2002). The direct conversion of carbon dioxide and water to produce organic products under such conditions can be considered as a form of "reverse combustion", chemically corresponding to the reverse process by which fossil fuels are typically consumed. Hypotheses on the origin-of-life on Earth present an interesting perspective on the hydrothermal conversion of CO_2. In particular, the serpentinisation of magnesium- and iron-rich rocks to produce H_2 by their alteration with water has been widely studied in this regard. Serpentinisation occurs in marine environments, such as mid-ocean ridges, ridge flanks and fracture zones. The hydrogen formed during serpentinisation can facilitate the reduction of CO_2 to produce CH_4 and higher hydrocarbons (McGlynn et al., 2020). It is noteworthy that the presence of CH_4 (Konn et al., 2015) and other hydrocarbons (Holm and Charlou, 2001; Botz et al., 2002) has been detected in oceanic ultramafic-hosted vent fluids. Sulphides and iron present in hydrothermal vents have been postulated to promote the synthesis of organics from CO_2, and therefore play a role in the origin of life on Earth (He et al., 2019).

In addition to oceanic observations, serpentinisation of olivine, an iron-containing mineral present in ultramafic

rocks, has also been investigated at laboratory scale to demonstrate the feasibility of producing organic compounds under hydrothermal conditions. Berndt *et al.* (Berndt et al., 1996) found that the oxidation of FeO present in olivine produced H_2 that reacts with CO_2 at 300°C and 500 bar to produce hydrocarbons such as methane, ethane and propane after 69 days. McCollom *et al.* (McCollom and Seewald, 2001) also investigated the serpentinisation of olivine at 350 bar. In those studies, formate was the principle organic species observed, with the only hydrocarbon formed being methane.

The role of iron in hydrothermal reactions of CO_2 has been widely studied as iron is widespread across the crust, mantle and core of Earth (Frey and Reed, 2012). Iron plays a twin role in these processes, acting both as a reductant and providing a surface-mediated reaction pathway of lower activation energy and thereby also acting as a solid catalyst. Guan *et al.* (Guan et al., 2003) studied different Fe-based materials, specifically Fe^0, Fe^0-K-Al and Fe^0-Cu-K-Al, for the synthesis of hydrocarbons and alcohols from CO_2. When Fe^0 was employed only CH_4 was formed, while the use of promoted-Fe materials favoured the formation of longer products such as propane, methanol and ethanol after 20 h reaction time. Hardy *et al.* (Hardy and Gillham, 1996) also investigated the behaviour of commercial Fe materials at room temperature, observing the formation of methane, ethane, ethene, propene and butenes after 144 h of reaction. Fe was also tested at higher temperatures, with hydrocarbons such as methane, ethane, ethene and propene were formed at 200°C from CO_2 in aqueous media (Takahashi et al., 2008). Phenol has also been observed as a product derived from gaseous CO_2 over Fe (Tian et al., 2010; Gomez et al., 2020), and in lower concentrations from $NaHCO_3$ as a CO_2 source, at 200°C (Tian et al., 2007) with Fe. In that work formic acid was produced as a minor co-product. Elsewhere, formic acid has been observed to be the major species produced from $NaHCO_3$ over Fe (Duo et al., 2016).

In addition to Fe, other materials have been investigated for the hydrothermal conversion of CO_2. For instance, Zn was shown to successfully act as a reductant to form formic acid (Jin et al., 2014; Roman-Gonzalez et al., 2018), while in the presence of both Zn and Cu methanol is formed (Huo et al., 2012; Liu et al., 2012). Ni was also studied in combination with Fe, producing formic acid in yields up to 15.6% under hydrothermal conditions (Wu et al., 2009). Al (Lyu et al., 2015) or biomass derivatives (Andérez-Fernández et al., 2018) have also been investigated as reductants, preferentially yielding methanol and formic acid respectively.

The aforementioned reactions are predominately selective to C_1 products such as methane, formic acid and methanol, all of which are valuable products. Methane is principally used as a fuel or to produce hydrogen (Michalkiewicz and Koren, 2015) and formic acid is used in the manufacture of textiles and pharmaceuticals, as a preservative and insecticide and also as an industrial source of carbon for the synthesis of other chemicals (Duo et al., 2016; Roman-Gonzalez et al., 2018). Formic acid has also attracted much interest as a potential hydrogen storage vector (Santos et al., 2021). The importance of methanol is based on its role in the production of formaldehyde, resins, dimethyl ether, methyl t-butyl ether, acetic acid, *etc.* Moreover, methanol can be used as an additive to gasoline and also as a potential fuel without modification of internal combustion engines (Baiker, 2000; Khirsariya and Mewada, 2013; Ganesh, 2016). In addition, methanol also represents a feasible and safe way to store energy. Owing to its potential to be produced from recycled CO_2 and to replace oil and gas as a platform chemical for the production of chemicals and fuels, methanol is the basis of the so called "Methanol Economy" (Olah, 2004; Ganesh, 2016).

In addition to C_1 products, we have previously reported the synthesis of oxygenates including cyclic ketones and phenol from CO_2 under hydrothermal conditions (Gomez et al., 2020). That study showed that the hydrothermal conversion of CO_2 is influenced by different reaction parameters which can be optimised to tailor the product distribution, *e.g.* to substances with a higher carbon number, and to enhance CO_2 conversion. In the present work, we have studied the effect of the reaction temperature, reaction time and the CO_2:H_2O mole ratio using Fe-based catalysts. Additionally, as the oxidation state of Fe in the catalyst may be critical in determining reaction progress, the influence of oxygen (in the form of air) in the reaction medium has been investigated.

Experimental section

Materials

CO_2 (purity 99.99%), H_2 (minimum purity 99.995%) and He (CP grade) purchased from BOC were used without further purification. The bulk iron materials employed as reductants and catalysts were Fe powder (≥99%, Sigma Aldrich, fine powder) and Fe_3O_4 (97% metal basis, Alfa Aesar, 350 mesh); these were used without further treatment or modification.

Reaction testing

To conduct the reaction, the reactor (100 ml internal volume EZE-Seal Reactor, Parker Autoclave Engineers®, manufactured from Hastelloy C) was loaded with 0.56 g of catalyst (either Fe or Fe_3O_4) and 7 ml of distilled water, unless otherwise stated. Gas chromatography mass spectrometry (GC-MS) (Shimadzu QP2010SE, DB1-MS column, 60 m length, 0.25 mm inner diameter, 0.25 μm film thickness) analysis of water samples prior to reaction, demonstrated that the presence of organic matter in the water was negligible. After loading catalyst and water, the reactor was twice flushed with CO_2 to eliminate air, before being pressurised to ~25 barg (CO_2:H_2O mole ratio =

0.26). This step was omitted when the influence of the CO_2:O_2 mole ratio was explored. In these studies, the reactor was instead filled with different amount of air prior to the addition of CO_2 but keeping the initial pressure equal to 25 barg. The temperature of the reactor was then increased to 300°C, unless otherwise stated. The time at which the impeller (600 rpm) was turned on was taken as the reaction start-time. At the end of the specified reaction time (4 h unless otherwise stated) a water-ice bath was placed around the reactor to quench the reaction. Gaseous products were extracted for analysis (*Product Analysis and Catalyst Characterisation Section*) and the system was then depressurised and liquid and solid materials were separated by vacuum filtration. The solids were rinsed with distilled water several times and subsequently dried overnight at ~110°C.

Selected experiments were conducted three times to calculate the dispersion coefficient, this is, the ratio of the standard deviation to the mean. Products with ≤3 carbons presented a dispersion of coefficient of 9% while products with ≥4 carbons had a coefficient of 3%.

Product analysis and catalyst characterisation

Gas phase products were analysed at ~22°C by mass spectrometry (MS) (HPR-20-QIC, Hiden Analytical). Details of the quantification of gas phase species are shown in the Supporting Information (*Introduction Section*). Analysis of the liquid products was performed by GC-MS on a Shimadzu QP2010SE equipped with a DB1-MS column, 60 m length, 0.25 mm inner diameter and 0.25 µm film thickness. 4-Methyl-2-pentanol (98%, Sigma Aldrich) was used as an internal standard in a ratio of 1 µL of internal standard to 1.5 ml of collected sample. Liquid products were quantified by calibration curves for the species identified. Details of the GC-MS analysis methods employed are provided in the Supporting Information (*Experimental Section*). CO_2 conversion (X_{CO2}) and product selectivity (S_i) were calculated according to Eqs 1, 2 respectively:

$$X_{CO2} = \left(n_{CO2,initial} - n_{CO2,final}/n_{CO2,initial}\right) \times 100 \quad (1)$$

$$S_i = \left(n_i/n_{CO2,initial} - n_{CO2,final}\right) \times 100 \quad (2)$$

where n_i is the number of moles of a given product formed and $n_{CO2,initial}$ and $n_{CO2,final}$ are the total number of moles of CO_2 present in both the gas and liquid phase at the beginning and end of the reaction, respectively.

Brunauer–Emmett–Teller (BET) surface areas of the Fe powder and Fe_3O_4 were determined by using a 3 Flex Micromeritics Surface Characterization instrument resulted the area of Fe_3O_4 of 7 m^{-2} g^{-1}. The surface area of bulk Fe powder was below the measurement range of the apparatus. The morphology of fresh and spent Fe_3O_4 after different reaction times was investigated by scanning electron microscopy (SEM) employing a Jeol JSM-6010 LA Analytical Scanning Electron Microscopy with an accelerating voltage ranging from 15 to 20 kV and a working distance of 12 mm. The physical structure of the iron oxide after reaction was also investigated by X-ray diffraction (XRD) to identify any changes in the composition of the catalyst. XRD patterns were recorded using a diffractometer (STOE STADI P) operated in transmission mode at a voltage of 20 kV and a current of 5 mA using STOE WinXPOW software. Data were collected at room temperature in the 2θ range from 5 to 39.98° with a step size of 0.020° with Mo-K_α radiation. The deposition of carbonaceous material (coke) on the catalysts was investigated by temperature-programmed oxidation (TPO), employing a pulse chemisorption system (ChemiSorb 2720, Micromeritics) equipped with a Eurotherm 2416 temperature controller. The TPO method consisted of flowing He at a flow rate of 25 ml min^{-1} over 30 min at room temperature in order to clean the catalyst surface. Then, the inert gas was substituted for the oxidation gas which comprised 5% O_2 and 95% He at the same flow rate. After 20 min the temperature was increased to 950°C at a rate of 10°C min^{-1} and this temperature was held for 30 min. The oxidation of unreacted Fe_3O_4 was investigated by thermogravimetric analysis (TGA). A TGA400 (PerkinElmer) was employed using the same conditions and temperature profile as TPO experiments.

Results and discussion

In order to gain a better understanding of the hydrothermal reaction of CO_2 and H_2O, and in particular the reaction mechanism and the factors affecting product distribution, the influence of: 1) reaction temperature (*Influence of Reaction Temperature Section*); 2) reaction time (*Influence of Reaction Time Section*); and 3) CO_2:O_2 ratio (*Influence of CO2:O2 ratio Section*) were investigated. In all the reactions investigated, the autogenous pressure increase resulted in a pressure during reaction of between 55 and 65 bar. Characterisation of the spent catalyst after reaction was also conducted in order to investigate any structural or morphological changes, and to establish the extent of any coking *(Characterisation of Spent Catalyst Section*).

Influence of reaction temperature

Previous work has demonstrated the viability of synthesising both short chained products, *e.g.* methanol, and longer-chained species, *e.g.* heptanal, at 300°C (Gomez et al., 2020). The hydrothermal conversion of CO_2 involves a complex network of competing series and parallel reactions of differing rates, and hence temperature is likely to play key role in controlling reaction selectivity. In addition, temperature changes will also influence

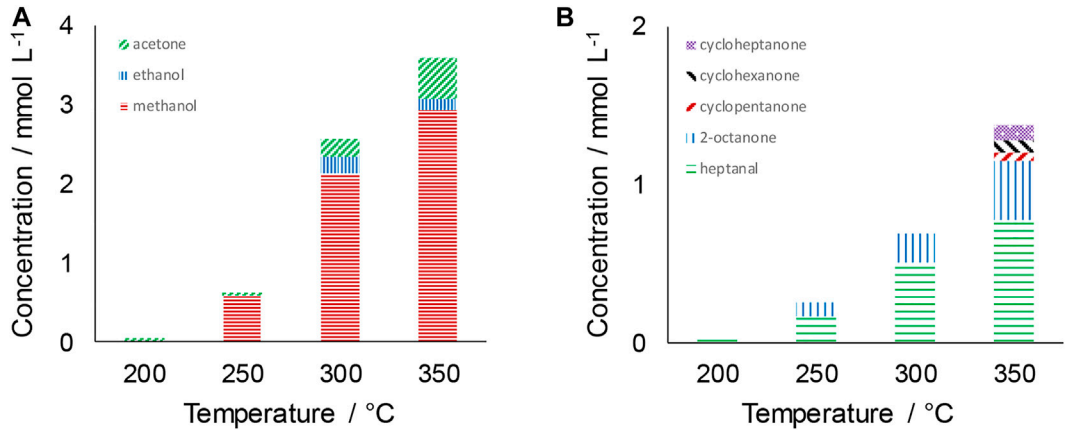

FIGURE 1
Distribution of liquid-phase products at different reaction temperatures. **(A)** ≤ C_3 products; **(B)** ≥ C_4 products. Reaction conditions: CO_2:H_2O mole ratio = 0.26; reaction time = 4 h; 0.56 g Fe.

TABLE 1 CO_2 conversion and gas phase composition at different reaction temperatures. Reaction conditions: CO_2:H_2O mole ratio = 0.26; reaction time = 4 h; 0.56 g Fe. "n.d." indicates that a species was not detected.

	Gas phase composition (mmol)								
T (°C)	X_{CO2} (%)	H_2	H_2O	CO_2	CH_4	CH_2O (formaldehyde)	CH_2O_2 (formic acid)	C_2H_4 (acetaldehyde)	C_2H_4 (ethane)
200	3.6	0.6	0.3	96.9	n.d	<0.1	<0.1	0.3	n.d
250	3.5	0.6	0.4	97.9	n.d	<0.1	<0.1	0.3	n.d
300	4.8	1.7	0.8	96.1	<0.1	<0.1	<0.1	0.3	n.d
350	3.5	1.9	0.6	94.0	<0.1	<0.1	<0.1	0.3	<0.1

the properties of sub-critical water, thereby altering hydrogen availability. Understanding these effects will facilitate the development of an understanding of the reaction mechanisms, and hence provide a basis for the future design of improved catalysts and processes.

The distribution of liquid products in the temperature range 200–350°C is shown in Figure 1 using Fe powder as the catalyst. Only very limited formation of products is observed at 200°C. At 250°C and above however, methanol is the major product. The concentration of methanol increases from 0.59 to 2.94 mmol L^{-1} between 250 and 350°C. Ethanol and acetone are also observed, although in much lower quantities than methanol. The concentration of acetone increases with increasing the reaction temperature, reaching 0.51 mmol L^{-1} at 350°C.

Considering ≥ C_4 products, Figure 1B, heptanal is seen to be the most abundant species. As per the trends observed with methanol, the concentration of heptanal significantly increased from 0.17 mmol L^{-1} at 250°C to 0.51 mmol L^{-1} at 300°C with a more moderate increase to 0.78 mmol L^{-1} at 350°C. 0.08 mmol L^{-1} 2-octanone was obtained at 250°C rising to 0.37 mmol L^{-1} at 350°C. Cyclic ketones from five to seven carbons were also detected in trace amounts at this highest temperature. The mechanism of formation of such longer-chained products has been hypothesized previously, with the initial step being the formation of either formate (HCOO) or carboxylate (COOH) species followed by step wise addition of CO_2 to increase chain length (Gomez et al., 2020).

In addition to liquid-phase products, analysis of the gas phase demonstrated the presence of products including H_2, formic acid, formaldehyde and acetaldehyde (Table 1). Above 300°C, hydrocarbons such as methane and ethene are also detected. CO_2 dominates the composition of the gas-phase and hence all other species, with the exception of H_2 at the highest reaction temperatures, are present in only trace quantities (<1% mole basis). Acetaldehyde is however

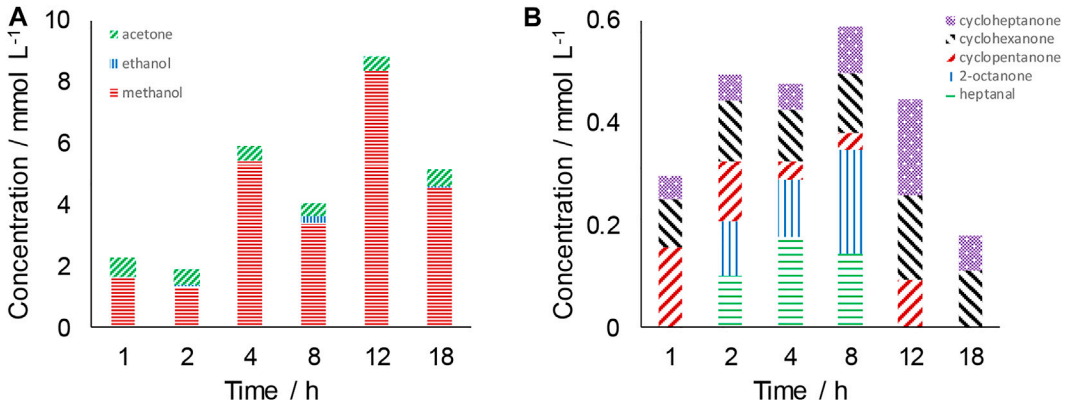

FIGURE 2
Distribution of liquid-phase products at reactions times ≤18 h **(A)** ≤ C_3 products; **(B)** ≥ C_4 products. Reaction conditions: T = 300°C; CO_2:H_2O mole ratio = 0.26; 0.56 g Fe_3O_4.

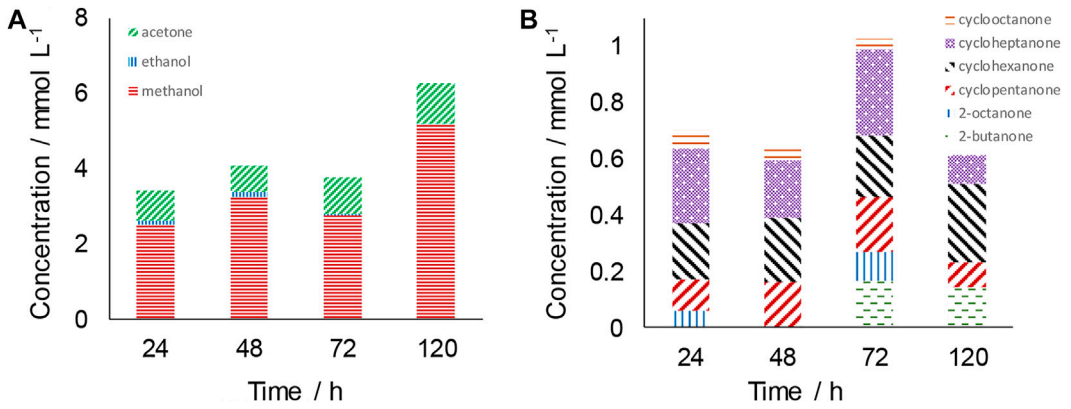

FIGURE 3
Distribution of liquid-phase products at reaction times ≥24 h **(A)** ≤ C_3 products; **(B)** ≥ C_4 products. Reaction conditions: T = 300°C; CO_2:H_2O mole ratio = 0.26; 0.56 g Fe_3O_4.

observed to be the most abundant organic product in the gas-phase at all temperatures.

Influence of reaction time

As with reaction temperature, the reaction time is expected to effect changes in product distribution, in particular as some of the species observed are expected to be the products of secondary, tertiary *etc.* reactions. Furthermore, observed changes in selectivity may evidence the relative difference in rates of any parallel reactions occurring. Previous work has shown product formation in this reaction after a period of 4 h with different catalysts, concluding that Fe_3O_4 showed the highest CO_2 conversion (Gomez et al., 2020). Herein reaction times of 1–120 h have been investigated using Fe_3O_4 as the catalyst. The reaction temperature was fixed at 300°C; this was shown in *Influence of Reaction Temperature Section* to result in significantly greater product formation than at 250°C and with reduced formation of minor by-products when compared to 350°C.

Figure 2A shows ≤ C_3 products formed at reaction times ≤18 h, and Figure 2B shows ≥ C_4 species synthesised also at reaction times ≤18 h. Inspection of Figure 2A shows that methanol was the major compound produced at all reaction times. The highest methanol concentration reached was greater than 8 mmol L^{-1} after 12 h of reaction (Figure 2A). The presence of acetone was also observed, with an approximately constant

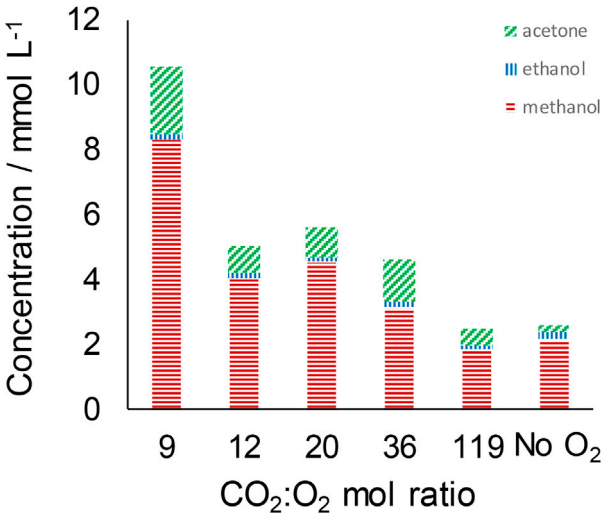

FIGURE 4
Distribution of liquid-phase ≤ C_3 products at different CO_2:O_2 mole ratios. Reaction conditions: T = 300°C; V_{H2O} = 7 ml; $P_{CO2+air}$ = 25 barg; reaction time = 4 h; 0.56 g Fe.

concentration of ~0.5 mmol L^{-1} during the first 18 h of reaction (Figure 2A). Ethanol was observed in trace concentrations in a number of experimental runs. Figure 3A shows that while methanol remains the predominant species at reaction times greater than 18 h, acetone concentration increases significantly at longer reaction times, reaching 1.1 mmol L^{-1} after 120 h.

Products of chain length ≥ C_4 are shown in Figures 2B, 3B for reaction times of ≤18 h and >18 h respectively. The species detected include straight-chained products such as heptanal and 2-octanone, and also cyclic ketones with rings of five, six and seven carbons. Heptanal and 2-octanone were only observed at 2, 4 and 8 h, whereas cyclic ketones appeared at all reaction times investigated. The highest cyclopentanone concentration achieved was ~0.15 mmol L^{-1} after 1 h of reaction. Cycloheptanone concentration tended to increase with increasing reaction time, reaching a maximum of 0.31 mmol L^{-1} after 72 h. At long times-on-stream (≥24 h) cycohexanone was also observed.

The distribution of the gas-phase products is shown in Supplementary Table S1. Calculated CO_2 conversions based on initial CO_2 concentration showed little variation with values ranging from 1.0 to 4.3%. These small variations can be explained by the nature of the reaction. This is a very complex system encompassing numerous equilibrium reactions. Therefore, CO_2 may react and decompose continuously with the reaction time. Furthermore, it should be taken into account that the value of CO_2 conversion not only refers to products formed but also to carbonaceous deposits on the catalyst surface as discussed in *Characterisation of Spent Catalyst Section*. In line with studies at different reaction temperatures (*Influence of Reaction Temperature Section*) organic products comprised <1 mol% of the gas phase, with CO_2 dominating the composition. Acetaldehyde was however detected at all reaction times investigated.

TABLE 2 Hydrogen and hydrocarbons detected in the gas phase at different CO_2:O_2 mole ratios. Reaction conditions: T = 300°C; V_{H2O} = 7 ml; $P_{CO2+air}$ = 25 barg; reaction time = 4 h; 0.56 g Fe.

CO_2:O_2 (mol)	H_2 (mmol)	CH_4 (μmol)	C_2H_4 (μmol)
9	1.0	16.8	38.1
12	1.3	14.2	33.3
20	1.4	23.2	43.4
36	1.4	27.3	48.9
119	2.5	15.1	20.3
No O_2	1.7	9.7	—

Influence of CO_2:O_2 ratio

Studies on the hydrothermal conversion of CO_2 are typically conducted in the absence of oxygen. Oxygen however has the potential to play a number of roles in the reaction; it may, for instance, facilitate the oxidation of the employed iron catalyst or may partake in the reaction directly. Therefore, the addition of O_2 (as air) at different CO_2:O_2 ratios has been investigated herein using Fe powder as the catalyst. Furthermore, the effect of including air in the reaction mixture is to reduce the partial pressure of CO_2. An equilibrium exists between carbon dioxide in the gas and H_2O-phases and hence changing p_{CO2} will alter the availability of the reactants and will also alter the pH of the system, with lower dissolved CO_2 concentrations in H_2O leading to decreased carbonic acid formation (Teramura et al., 2017).

CO_2:O_2 mole ratios of 9, 12, 20, 36 and 119 were investigated. Figure 4 shows that the inclusion of oxygen in the reaction mixture, and the corresponding reduction in CO_2 partial pressure, is correlated with an increase in the production of ≤ C_3 products. The maximum methanol concentration observed (8.3 mmol L^{-1}) occurs at the lowest CO_2:O_2 ratio investigated of 9 (corresponding to ~2.1 bar O_2). Acetone shows similarly enhanced production with a concentration ~10-fold higher than that observed in the absence of O_2 at this CO_2:O_2 ratio. In contrast, the presence of air, and hence reduced p_{CO2}, results in a reduction in the formation of ≥ C_4 species. For instance, pentanal, heptanal, cyclohexanone and 2-octanone, all of which are observed in the absence of O_2, were only detected at the highest CO_2:O_2 ratio investigated of 119.

As with the other reaction parameters investigated in this work (influence of the reaction temperature and reaction time), the gas-phase is dominated by CO_2, with the organic products detected (Supplementary Table S2) representing ≤1 mol%. Acetaldehyde was however observed at all ratios studied. CO

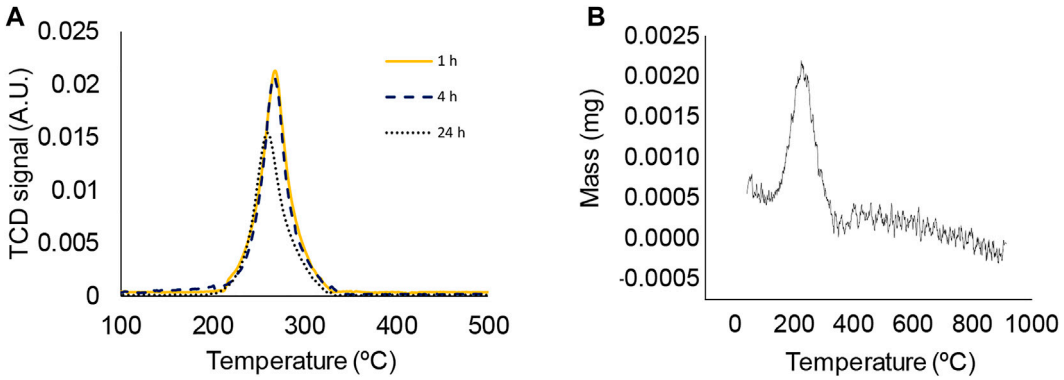

FIGURE 5
(A) TPO profile of spent Fe_3O_4 catalyst after different reaction times. Reaction conditions: T = 300°C; CO_2:H_2O mole ratio = 0.26; 0.56 g Fe_3O_4. Mass of spent catalyst employed in TPO analysis = 30–40 mg. **(B)** DTG analysis of the oxidation of fresh Fe_3O_4 employing an intial mass of 10.4 mg Fe_3O_4.

in contrast, was only observed at the lowest CO_2:O_2 mole ratio of 9, in a relatively low concentration corresponding to ~33 μmol. At this ratio, formic acid was not detected, therefore CO could be formed *via* the decomposition of formic acid into CO, CO_2 and H_2 as formic acid is known to be unstable under hydrothermal conditions (Yu and Savage, 1998). Additionally, formic acid may also be an intermediate in the formation of CH_4 (Zhong et al., 2019b). Under aerobic conditions, the quantity of H_2 in the gas phase gradually increased with increasing CO_2:O_2 mole ratios (Table 2). Notably, in the absence of air the concentration of H_2 was lower when compared to the highest investigated CO_2:O_2 mole ratio of 119, equivalent to 0.21 bar O_2. This observation correlates well with previous research on utilizing $NaHCO_3$ as the CO_2 source in hydrothermal reactions employing Fe a reductant, where increased $NaHCO_3$ concentrations resulted in higher H_2 yields. (Duo et al., 2016; Jiang et al., 2017). Those works hypothesised that Fe was converted to $FeCO_3$, which in turn reacted to FeO, with the evolution of CO_2. FeO can then react with water to form Fe_3O_4, generating H_2 as a co-product. The formed CO_2 can react with additional $FeCO_3$ ultimately generating more H_2 from water.

Characterisation of spent catalyst

Spent Fe_3O_4 was characterised after different times-on-stream by temperature-programmed oxidation (TPO), scanning electron microscopy (SEM) and X-ray diffraction (XRD). To investigate the evolution of the catalyst during the first 24 h of reaction, TPO analysis was conducted for spent catalysts after 1, 4 and 24 h of reaction to investigate if significant quantities of carbon deposits are present on the catalyst and if so, how these change with time-on-stream. The TPO profiles for the three reaction times evaluated show very similar characteristics with a single symmetric peak centred at ~260°C (Figure 5A). This low temperature peak is in the region expected for amorphous carbon species (Bayraktar and Kugler, 2002; Gomez Sanz et al., 2015; Gomez Sanz et al., 2016). However, complementary TGA measurements of fresh Fe_3O_4 carried out under oxidative conditions and employing the same temperature profile as TPO experiments indicate that this peak coincides with the temperature at which Fe_3O_4 is oxidized to Fe_2O_3. The first derivative of the TGA plot (i.e. differential thermogravimetric analysis (DTG)) is shown in Figure 5B. The oxidation of Fe_3O_4 during TPO measurements therefore obscures the identification of any carbon deposits that may be present. There is a slight shift in peak position towards lower temperatures with increasing times-on-stream and a reduction in peak intensity for the sample from the 24 h reaction. This may indicate that some surface oxidation of the catalyst has taken place during reaction.

Morphological changes in the catalyst during reaction were investigated by SEM (Figure 6). Both fresh and spent catalysts existed as agglomerates of small grains. The micrographs are suggestive of an increase in particle density with increasing reaction time. Indeed, at the longest reaction times (Figures 6E,F), the particles appeared more compacted. These changes in the catalysts may have been caused by the deposition of carbonaceous material and the hydrothermal reaction conditions.

Based on the observations from SEM studies and in order to evaluate if the reaction time promoted transformations in the catalyst crystalline phase, the XRD pattern of spent Fe_3O_4 after 120 h of reaction time was recorded and is shown in Figure 7. This pattern was analysed with PDF-4+ 2016 software. The observed peaks after 120 h corresponded to the typical XRD peaks of Fe_3O_4, as confirmed by comparison to a reference XRD pattern of Fe_3O_4 obtained from the RRUFF database (RRUFF, 2022). Reaction therefore does not appear to promote changes in the crystalline phase of the catalyst even at extended reaction times.

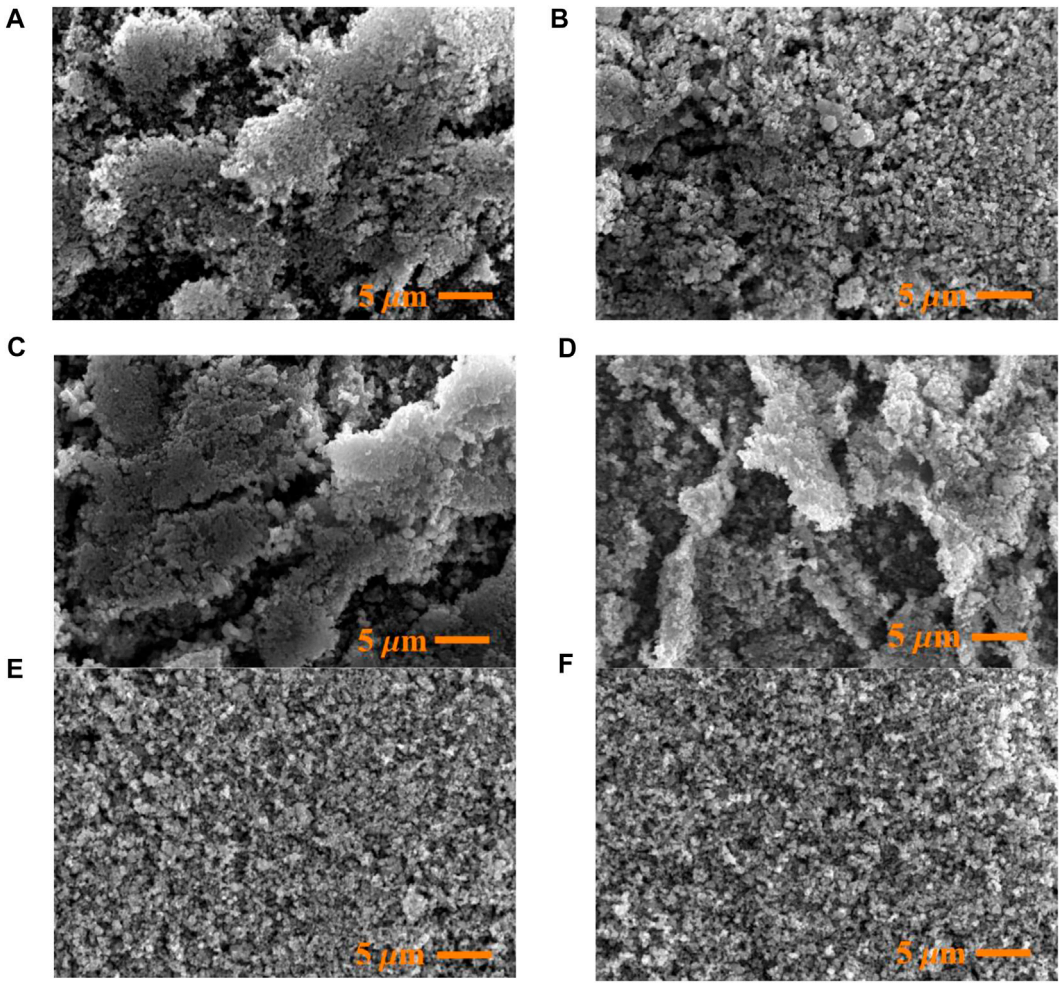

FIGURE 6
Fresh and post-reaction SEM images of catalysts employed in the hydrothermal reduction of CO_2 at different reaction times: **(A)** fresh catalyst; **(B)** 1 h; **(C)** 4 h; **(D)** 8 h; **(E)** 18 h; **(F)** 120 h.

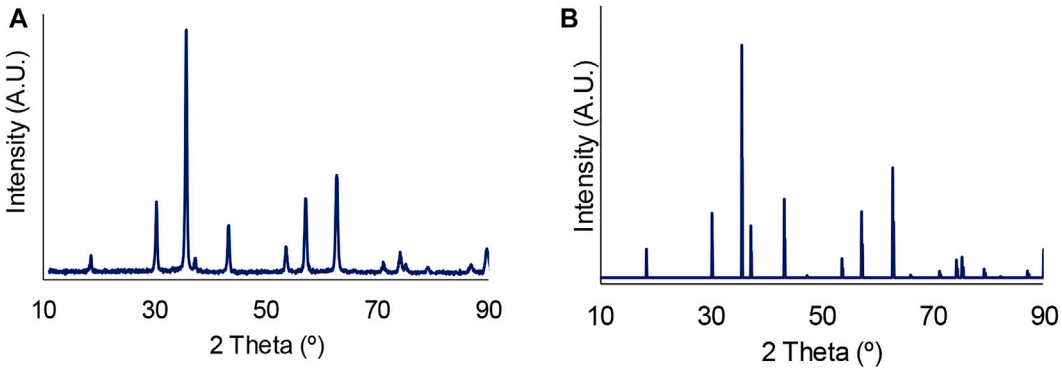

FIGURE 7
(A) XRD pattern for spent Fe_3O_4 after 120 h of reaction time; **(B)** Reference XRD pattern for Fe_3O_4 from RRUFF database, RRUFF id R061111.2 (RRUFF, 2022).

Reaction mechanism

As described in *Reaction testing*, reactions were carried out in a Hastelloy C reactor. Hastelloy C contains 58.6% Ni and the conversion of CO_2 into oxygenates over Ni powders has been previously reported (Takahashi et al., 2006; Wu et al., 2009). Therefore, the influence of the reactor walls on reaction was investigated. CO_2 and H_2O in a mole ratio of 0.26 were reacted at 300°C for 4 h in the absence of a catalyst. Approximately 1 mmol/L of methanol and trace amounts of acetone were detected. It cannot however be unambiguously concluded from this result that the reactor wall plays a catalytic role in the reaction as the formation of organics could also be ascribed to the elevated reaction temperature and pressure. The quantities of organic products obtained are however significantly lower than those observed in the presence of iron materials at these conditions (*Influence of Reaction Temperature Section*), confirming the positive role played by iron in enhancing CO_2 conversion.

Figure 1 demonstrated that increasing reaction temperature led to an increase in the quantity of liquid-phase products produced. Furthermore, a broader range of products was detected as the temperature increased, with cyclic ketones ranging from five to seven carbons detected in trace amounts at 350°C. The variation in product distribution with time over Fe_3O_4 is greater still than the variation with reaction temperature observed over Fe. In all cases however it is apparent that methanol is the major liquid-phase product identified.

While the synthesis of methanol *via* CO_2 hydrogenation in gas/solid reactions is well studied and the mechanism widely investigated (Bowker, 2019; Murthy et al., 2021; Numpilai et al., 2021), the mechanism of methanol production from CO_2 and H_2O under hydrothermal conditions is much less well understood. Huo *et al.* (Huo et al., 2012) proposed that H^+ concentration in the reaction media plays a key role in determining the yield of methanol obtained, observing that high H^+ concentrations and hence high acidity correlated with higher methanol yields. In the present work, high reaction temperatures are associated with increased methanol production. In addition to providing increased energy to facilitate CO_2 activation and conversion, higher temperatures also increase the extent of H_2O dissociation, thereby increasing the availability of H^+ in the reaction medium. This may therefore also play a role in explaining the increase in methanol production.

Considering the influence of reaction time on the product distribution observed over Fe_3O_4, Figures 2, 3 show that the rise in methanol concentration before 12 h on-stream and the decline in methanol concentration after 12 h on-stream is not monotonic. This may therefore suggest that methanol continuously forms and decomposes or further reacts over the timescale of the hydrothermal reaction. In addition to methanol, longer-chained linear organic products were also produced. Among these, 2-butanone, heptanal and 2-octanone were the major species detected. At shorter reaction times, 2-butanone was detected only at 2 h of reaction time and in very low concentrations, specifically 0.08 mmol L^{-1}. Higher concentrations were observed at longer times-on-stream with 0.17 mmol L^{-1} and 0.14 mmol L^{-1} detected at 72 and 120 h respectively. Heptanal was observed only at reaction times of 8 h or below, reaching its highest concentration of 0.18 mmol L^{-1} at 4 h. The presence or absence of 2-octanone varies at different reaction times. This and other fluctuations in the concentration of products observed reinforces the hypothesis that the conversion of CO_2 under hydrothermal conditions is a complex system with numerous competing reactions, where different species form and decompose in series and parallel reactions.

The same conclusion can be reached by observing the concentration of gas phase products, specifically H_2, methane and ethene, at different reaction times as shown in Supplementary Table S1. There is no clear trend in the quantity of H_2 detected after reaction; this ranges from <0.1 to 0.7 mmol. Note that the quantity of hydrogen observed is less than the total amount produced during reaction as H_2 has also been consumed in the hydrogenation of CO_2 to organic product molecules, specifically hydrocarbons and oxygenates. Methane and ethene were both observed at shorter reaction times, however neither were observed at times on stream in excess of 48 h. Methane production persists for longer times-on-stream as compared to ethene production.

A closer look to the formation of short-chained liquid phase products with temperature provides clearer insights into aspects of the reaction mechanism and which products are formed through the same, or different, mechanistic pathways. Notably, not only does the absolute concentration of acetone increase with increasing temperature, but it also comprises an ever greater fraction of > C_1 species formed. This increases from 14% at 250°C, to 19% at 300°C and 25% at 350°C. In contrast, the percentage of methanol among the detected products shows little variance with reaction temperature, decreasing from 67% of the detected liquid-phase species at 250°C, to 65% at 300°C and 59% at 350°C. Therefore, the acetone:methanol ratio increases ~2.6-fold over this temperature range. A much closer relationship is observed between the concentrations of acetone and ethanol produced. In the temperature range 300–350°C, the increase in acetone production is mirrored by a decrease in the synthesis of ethanol. A similar trend is observed in studies investigating the influence of CO_2:O_2 ratio where the reaction shifts in favour of ethanol (*vs.* acetone) as the CO_2:O_2 ratio increases. Specifically, the acetone:ethanol ratio decreases monotonically from 18.2 at a CO_2:O_2 ratio of 9 to 4.4 at a CO_2:O_2 ratio of 119 and 1.0 in the absence of air.

These trends observed at different temperatures and for different CO_2:O_2 mole ratios provide evidence to suggest that ethanol and acetone production are to some extent inversely

correlated. The production of these is not coupled to the synthesis of methanol, suggesting that ethanol and acetone may be competitively produced in one reaction pathway, while methanol is produced in an independent, parallel, pathway. The synthesis of ethanol directly from CO_2 and H_2O without passing through methanol as an intermediate has been proposed previously (Chen et al., 2017). Moreover, in previous studies of gas-solid reactions (*i.e.* not under hydrothermal conditions) (Rodrigues et al., 2013; de Lima et al., 2017; Rodrigues et al., 2017; Silva-Calpa et al., 2017) it was proposed that acetone was produced from the catalytic conversion of ethanol *via* acetaldehyde as an intermediate. Specifically, acetaldehyde is formed from the dehydrogenation of ethanol which has previously been shown to be promoted by zero-valent metal sites (Rodrigues et al., 2013). Acetaldehyde then generates acetate species which condense to form acetone. Notably, zero-valent metal sites can also adsorb and dissociate water (Hardy and Gillham, 1996). In all reaction systems investigated in the present work, acetaldehyde was detected in the gas-phase which may support the hypothesis that it is an intermediate in acetone production. The relative decrease in acetone production as compared to ethanol production with increasing CO_2:O_2 ratio may be a consequence of factors such as a lower overall extent of reaction, changes in pH or by equilibrium effects as CO_2 is a by-product from acetate condensation (Rodrigues et al., 2013).

The formation of acetaldehyde under hydrothermal conditions along with oxygenates such as ethanol and acetic acid by the reduction of CO_2 with Fe_3O_4 has also been reported by Chen and Bhanemann (Chen and Bahnemann, 2000) in the temperature range 100 to 350°C. They observed an inverse relationship between the production of ethanol and acetic acid. Acetic acid can be produced by the oxidation of acetaldehyde over heterogeneous catalysts *via* an acetate pathway or by the formation of an acetyl and a hydroxyl on the catalyst surface, the former route being more energetically favourable (Han et al., 2019).

The observations from the studies in the present work have therefore yielded a number of insights into the hydrothermal conversion of CO_2. The hypotheses formed provide a framework within which to conduct future mechanistic investigations, for example spiking the reaction with key hypothesized reaction intermediates. This will provide a fuller understanding of this complex reaction system and thereby to facilitate the optimisation of both reaction conditions and catalyst design.

Conclusion

The influence of reaction conditions on the hydrothermal conversion of CO_2 in the absence of gas-phase H_2 has been demonstrated, focusing on the influence of reaction temperature, reaction time and CO_2:O_2 mole ratio. Methanol is shown to be the major product formed, with a concentration of 8 mmol L^{-1} after 12 h of reaction. Other species up to C_8, including C_5-C_7 cyclic ketones are also observed. Increasing temperature increases the yield of methanol, correlated with increased energy in the system and hence increased activity, but also with greater availability of H^+ through enhanced H_2O dissociation. The presence of oxygen also increases methanol production. Acetone production is also enhanced by the presence of O_2, increasing 10-fold at a CO_2:O_2 ratio of 9 as compared to that observed in the absence of O_2. Acetone is proposed to be formed as a result of ethanol dehydrogenation *via* an acetaldehyde intermediate. Further optimization of the reaction system, and tailoring to specific desired products, is possible through, *e.g.*, improvements in catalysts/reductants and further insights into the complex reaction mechanisms.

Data availability statement

The original contributions presented in the study are included in the article/Supplementary Material, further inquiries can be directed to the corresponding author.

Author contributions

LQ-G—Conceptualization, Methodology, Investigation, Writing—Original Draft, Writing—Review and Editing; MC—Investigation; AS—Investigation; AA-S—Investigation; JM—Conceptualization, Methodology, Resources, Writing—Review and Editing, Supervision, Project administration, Funding acquisition.

Funding

Elements of the data presented herein were acquired with the support of the Engineering and Physical Sciences Research Council (EPSRC) "4CU" programme grant, aimed at sustainable conversion of carbon dioxide into fuels, led by The University of Sheffield and carried out in collaboration with University College London, the University of Manchester, and Queen's University Belfast.

Acknowledgments

The authors acknowledge the EPSRC for supporting this work financially (Grant No. EP/K001329/1). Dr. Alan Dunbar (University of Sheffield) is thanked for his support in obtaining SEM micrographs. Habib Suleymanov and Julie Swales (University of Sheffield) are acknowledge for their supported in conducting TGA measurements of Fe_3O_4. For the purpose of open access,

Conflict of interest

The authors declare that the research was conducted in the absence of any commercial or financial relationships that could be construed as a potential conflict of interest.

Publisher's note

Supplementary material

The Supplementary Material for this article can be found online at: https://www.frontiersin.org/articles/10.3389/fenrg.2022.917943/full#supplementary-material

SUPPLEMENTARY TABLE S1
CO_2 conversion and gas phase composition at different reaction times. Reaction conditions: T=300°C; CO_2:H_2O=0.26; 0.56 g Fe_3O_4. "n.d." indicates that a species was not detected.

SUPPLEMENTARY TABLE S2
CO_2 conversion and gas phase composition at different CO_2:air mole ratios. Reaction conditions: T=300°C; V_{H2O}=7 mL; $P_{CO2+air}$=25 barg; reaction time = 4 h; 0.56 g Fe. "n.d." indicates that a species was not detected.

References

Akiya, N., and Savage, P. E. (2002). Roles of water for chemical reactions in high-temperature water. *Chem. Rev.* 102, 2725–2750. doi:10.1021/cr000668w

Andérez-Fernández, M., Pérez, E., Martín, A., and Bermejo, M. D. (2018). Hydrothermal CO2 reduction using biomass derivatives as reductants. *J. Supercrit. Fluids* 133, 658–664. doi:10.1016/J.SUPFLU.2017.10.010

Baiker, A. (2000). Utilization of carbon dioxide in heterogeneous catalytic synthesis. *Appl. Organomet. Chem.* 14, 751–762. doi:10.1002/1099-0739(200012)14:12<751::AID-AOC85>3.0.CO;2-J

Bayraktar, O., and Kugler, E. L. (2002). Characterization of coke on equilibrium fluid catalytic cracking catalysts by temperature-programmed oxidation. *Appl. Catal. A General* 233, 197–213. doi:10.1016/S0926-860X(02)00142-4

Berndt, M. E., Allen, D. E., and Seyfried, W. E. (1996). Reduction of CO2 during serpentinization of olivine at 300°C and 500 bar. *Geology* 24, 351–354. doi:10.1130/0091-7613(1996)024<0351:ROCDSO>2.3.CO;2

Botz, R., Wehner, H., Schmitt, M., Worthington, T. J., Schmidt, M., and Stoffers, P. (2002). Thermogenic hydrocarbons from the offshore Calypso hydrothermal field, Bay of Plenty, New Zealand. *Chem. Geol.* 186, 235–248. doi:10.1016/S0009-2541(01)00418-1

Bowker, M. (2019). Methanol synthesis from CO2 hydrogenation. *ChemCatChem* 11, 4238–4246. doi:10.1002/cctc.201900401

Chen, Q. W., and Bahnemann, D. W. (2000). Reduction of carbon dioxide by magnetite: implications for the primordial synthesis of organic molecules. *J. Am. Chem. Soc.* 122, 970–971. doi:10.1021/JA991278Y

Chen, X., Abdullah, H., Kuo, D-H., Huang, H-N., and Fang, C-C. (2017). Abiotic synthesis with the C-C bond formation in ethanol from CO2 over (Cu, M)(O, S) catalysts with M = Ni, Sn, and Co. *Sci. Rep.* 7, 10094. doi:10.1038/s41598-017-10705-3

De Guido, G., Compagnoni, M., Pellegrini, L. A., and Rossetti, I. (2018). Mature versus emerging technologies for CO2 capture in power plants: key open issues in post-combustion amine scrubbing and in chemical looping combustion. *Front. Chem. Sci. Eng.* 12, 315–325. doi:10.1007/s11705-017-1698-z

de Lima, A. F. F., Zonetti, P. C., Rodrigues, C. P., and Appel, L. G. (2017). The first step of the propylene generation from renewable raw material: acetone from ethanol employing CeO2 doped by Ag. *Catal. Today* 279, 252–259. doi:10.1016/j.cattod.2016.04.038

Duo, J., Jin, F., Wang, Y., Zhong, H., Lyu, L., Yao, G., et al. (2016). NaHCO3-enhanced hydrogen production from water with Fe and *in situ* highly efficient and autocatalytic NaHCO3 reduction into formic acid. *Chem. Commun.* 52, 3316–3319. doi:10.1039/c5cc09611a

Frey, P. A., and Reed, G. H. (2012). The ubiquity of iron. *ACS Chem. Biol.* 7, 1477–1481. doi:10.1021/cb300323q

Ganesh, I. (2016). Electrochemical conversion of carbon dioxide into renewable fuel chemicals - the role of nanomaterials and the commercialization. *Renew. Sustain. Energy Rev.* 59, 1269–1297. doi:10.1016/j.rser.2016.01.026

Global Monitoring Laboratory (2021). *Trends in atmospheric carbon dioxide*. Available at: https://gml.noaa.gov/ccgg/trends/ (Accessed April, 2022).

Gomez, L. Q., Shehab, A. K., Al-Shathr, A., Ingram, W., Konstantinova, M., Cumming, D., et al. (2020). H2-free synthesis of aromatic, cyclic and linear oxygenates from CO2. *ChemSusChem* 13, 647–658. doi:10.1002/cssc.201902340

Gomez Sanz, S., McMillan, L., McGregor, J., Zeitler, J. A., Al-Yassir, N., Al-Khattaf, S., et al. (2015). A new perspective on catalytic dehydrogenation of ethylbenzene: the influence of side-reactions on catalytic performance. *Catal. Sci. Technol.* 5, 3782–3797. doi:10.1039/c5cy00457h

Gomez Sanz, S., McMillan, L., McGregor, J., Zeitler, J. A., Al-Yassir, N., Al-Khattaf, S., et al. (2016). The enhancement of the catalytic performance of CrO x/Al 2 O 3 catalysts for ethylbenzene dehydrogenation through tailored coke deposition. *Catal. Sci. Technol.* 6, 1120–1133. doi:10.1039/C5CY01157D

Guan, G., Kida, T., Ma, T., Kimura, K., Abe, E., and Yoshida, A. (2003). Reduction of aqueous CO 2 at ambient temperature using zero-valent iron-based composites. *Green Chem.* 5, 630–634. doi:10.1039/b304395a

Han, S., Shin, K., Henkelman, G., and Mullins, C. B. (2019). Selective oxidation of acetaldehyde to acetic acid on Pd-Au bimetallic model catalysts. *ACS Catal.* 9, 4360–4368. doi:10.1021/acscatal.9b00079

Hardy, L. I., and Gillham, R. W. (1996). Formation of hydrocarbons from the reduction of aqueous CO2 by zero-valent iron. *Environ. Sci. Technol.* 30, 57–65. doi:10.1021/es950054m

He, R., Hu, B., Zhong, H., Jin, F., Fan, J., Hu, Y. H., et al. (2019). Reduction of CO2 with H2S in a simulated deep-sea hydrothermal vent system. *Chem. Commun.* 55, 1056–1059. doi:10.1039/c8cc08075e

Holm, N. G., and Charlou, J. L. (2001). Initial indications of abiotic formation of hydrocarbons in the rainbow ultramafic hydrothermal system, Mid-Atlantic Ridge. *Earth Planet. Sci. Lett.* 191, 1–8. doi:10.1016/S0012-821X(01)00397-1

Huo, Z., Hu, M., Zeng, X., Yun, J., and Jin, F. (2012). Catalytic reduction of carbon dioxide into methanol over copper under hydrothermal conditions. *Catal. Today* 194, 25–29. doi:10.1016/j.cattod.2012.06.013

Jiang, C., Zhong, H., Yao, G., Duo, J., and Jin, F. (2017). One-step water splitting and NaHCO3 reduction into hydrogen storage material of formate with Fe as the reductant under hydrothermal conditions. *Int. J. Hydrogen Energy* 42, 17476–17487. doi:10.1016/J.IJHYDENE.2017.03.022

Jin, F., Zeng, X., Liu, J., Jin, Y., Wang, L., Zhong, H., et al. (2014). Highly efficient and autocatalytic H2O dissociation for CO2 reduction into formic acid with zinc. *Sci. Rep.* 4, 4503. doi:10.1038/srep04503

Jovan, D. J., and Dolanc, G. (2020). Can green hydrogen production be economically viable under current market conditions. *Energies* 13, 6599. doi:10.3390/en13246599

Keith, D. W., Holmes, G., Angelo, St.D., and Heidel, K. (2018). A process for capturing CO2 from the atmosphere. *Joule* 2, 1573–1594. doi:10.1016/j.joule.2018.05.006

Khirsariya, P., and Mewada, R. K. (2013). Single step oxidation of methane to methanol - towards better understanding. *Procedia Eng.* 51, 409–415. doi:10.1016/j.proeng.2013.01.057

Konn, C., Charlou, J. L., Holm, N. G., and Mousis, O. (2015). The production of methane, hydrogen, and organic compounds in ultramafic-hosted hydrothermal vents of the mid-atlantic ridge. *Astrobiology* 15, 381–399. doi:10.1089/ast.2014.1198

Liu, J., Zeng, X., Cheng, M., Yun, J., Li, Q., Jing, Z., et al. (2012). Reduction of formic acid to methanol under hydrothermal conditions in the presence of Cu and Zn. *Bioresour. Technol.* 114, 658–662. doi:10.1016/j.biortech.2012.03.032

Lyu, L., Jin, F., Zhong, H., Chen, H., and Yao, G. (2015). A novel approach to reduction of CO2 into methanol by water splitting with aluminum over a copper catalyst. *RSC Adv.* 5, 31450–31453. doi:10.1039/c5ra02872h

Mac Dowell, N., Fennell, P. S., Shah, N., and Maitland, G. C. (2017). The role of CO2 capture and utilization in mitigating climate change. *Nat. Clim. Chang.* 7, 243–249. doi:10.1038/nclimate3231

McCollom, T. M., and Seewald, J. S. (2001). A reassessment of the potential for reduction of dissolved CO2 to hydrocarbons during serpentinization of olivine. *Geochim. Cosmochim. Acta* 65, 3769–3778. doi:10.1016/S0016-7037(01)00655-X

McGlynn, S. E., Glass, J. B., Johnson-Finn, K., Klein, F., Sanden, S. A., Schrenk, M. O., et al. (2020). Hydrogenation reactions of carbon on Earth: Linking methane, margarine, and life. *Am. Mineral.* 105, 599–608. doi:10.2138/am-2020-6928CCBYNCND

Michalkiewicz, B., and Koren, Z. C. (2015). Zeolite membranes for hydrogen production from natural gas: state of the art. *J. Porous Mat.* 22, 635–646. doi:10.1007/s10934-015-9936-6

Murthy, P. S., Liang, W., Jiang, Y., and Huang, J. (2021). Cu-based nanocatalysts for CO2Hydrogenation to methanol. *Energy Fuels* 35, 8558–8584. doi:10.1021/acs.energyfuels.1c00625

Numpilai, T., Kidkhunthod, P., Cheng, C. K., Wattanakit, C., Chareonpanich, M., Limtrakul, J., et al. (2021). CO2 hydrogenation to methanol at high reaction temperatures over In2O3/ZrO2 catalysts: influence of calcination temperatures of ZrO2 support. *Catal. Today* 375, 298–306. doi:10.1016/j.cattod.2020.03.011

Olah, G. A. (2004). After oil and gas: methanol economy. *Catal. Lett.* 93, 1–2. doi:10.1023/b:catl.0000017043.93210.9c

Omodolor, I. S., Otor, H. O., Andonegui, J. A., Allen, B. J., and Alba-Rubio, A. C. (2020). Dual-function materials for CO 2 capture and conversion: a Review. *Ind. Eng. Chem. Res.* 59, 17612–17631. doi:10.1021/acs.iecr.0c02218

Rodrigues, C. P., Zonetti, P. da C., and Appel, L. G. (2017). Chemicals from ethanol: the acetone synthesis from ethanol employing Ce0.75Zr0.25O2, ZrO2 and Cu/ZnO/Al2O3. *Chem. Cent. J.* 11, 30. doi:10.1186/s13065-017-0249-5

Rodrigues, C. P., Zonetti, P. C., Silva, C. G., Gaspar, A. B., and Appel, L. G. (2013). Chemicals from ethanol - the acetone one-pot synthesis. *Appl. Catal. A General* 458, 111–118. doi:10.1016/j.apcata.2013.03.028

Roman-Gonzalez, D., Moro, A., Burgoa, F., Pérez, E., Nieto-Márquez, A., Martín, Á., et al. (2018). 2Hydrothermal CO2 conversion using zinc as reductant: Batch reaction, modeling and parametric analysisof the process. *J. Supercrit. Fluids* 140, 320–328. doi:10.1016/j.supflu.2018.07.003

RRUFF (2022). Magnetite R061111 - RRUFF database: Raman, X-ray, infrared, and chemistry. Available at: https://rruff.info/magnetite/display=default/R061111 (accessed June 7, 2022).

Santos, J. L., Megías-Sayago, C., Ivanova, S., Centeno, M. Á., and Odriozola, J. A. (2021). Functionalized biochars as supports for Pd/C catalysts for efficient hydrogen production from formic acid. *Appl. Catal. B Environ.* 282, 119615. doi:10.1016/j.apcatb.2020.119615

Silva-Calpa, L. D. R., Zonetti, P. C., de Oliveira, D. C., de Avillez, R. R., and Appel, L. G. (2017). Acetone from ethanol employing ZnxZr1−xO2−y. *Catal. Today* 289, 264–272. doi:10.1016/j.cattod.2016.09.011

Stocker, T., Plattner, G-K., Tignor, M., Allen, S., Boschung, J., Nauels, A., et al. (2013). *IPCC, 2013: climate change 2013: the physical science basis. contribution of working group I to the fifth assessment report of the intergovernmental panel on climate change*. United Kingdom and New York, NY: Cambridge University Press.

Styring, P., Jansen, D., de Coninck, H., Reith, H., and Armstrong, K. (2011). *Carbon capture and utilisation in the green economy*. York: Centre for Low Carbon Futures.

Takahashi, H., Kori, T., Onoki, T., Tohji, K., and Yamasaki, N. (2008). Hydrothermal processing of metal based compounds and carbon dioxide for the synthesis of organic compounds. *J. Mat. Sci.* 43, 2487–2491. doi:10.1007/s10853-007-2041-8

Takahashi, H., Liu, L. H., Yashiro, Y., Ioku, K., Bignall, G., Yamasaki, N., et al. (2006). CO2 reduction using hydrothermal method for the selective formation of organic compounds. *J. Mat. Sci.* 41, 1585–1589. doi:10.1007/s10853-006-4649-5

Teramura, K., Hori, K., Terao, Y., Huang, Z., Iguchi, S., Wang, Z., et al. (2017). Which is an intermediate species for photocatalytic conversion of CO2 by H2O as the electron donor: CO2 molecule, carbonic acid, bicarbonate, or carbonate ions? *J. Phys. Chem. C* 121, 8711–8721. doi:10.1021/acs.jpcc.6b12809

Tian, G., He, C., Chen, Y., Yuan, H. M., Liu, Z. W., Shi, Z., et al. (2010). Hydrothermal reactions from carbon dioxide to phenol. *ChemSusChem* 3, 323–324. doi:10.1002/cssc.200900274

Tian, G., Yuan, H., Mu, Y., He, C., and Feng, S. (2007). Hydrothermal reactions from sodium hydrogen carbonate to phenol. *Org. Lett.* 9, 2019–2021. doi:10.1021/ol070597o

Wu, B., Gao, Y., Jin, F., Cao, J., Du, Y., and Zhang, Y. (2009). Catalytic conversion of NaHCO3 into formic acid in mild hydrothermal conditions for CO2 utilization. *Catal. Today* 148, 405–410. doi:10.1016/j.cattod.2009.08.012

Yu, J., and Savage, P. E. (1998). Decomposition of formic acid under hydrothermal conditions. *Ind. Eng. Chem. Res.* 37, 2–10. doi:10.1021/ie970182e

Zhong, H., Wang, L., Yang, Y., He, R., Jing, Z., and Jin, F. (2019). Ni and Zn/ZnO synergistically catalyzed reduction of bicarbonate into formate with water splitting. *ACS Appl. Mat. Interfaces* 11, 42149–42155. doi:10.1021/acsami.9b14039

Zhong, H., Yao, G., Cui, X., Yan, P., Wang, X., and Jin, F. (2019). Selective conversion of carbon dioxide into methane with a 98% yield on an *in situ* formed Ni nanoparticle catalyst in water. *Chem. Eng. J.* 357, 421–427. doi:10.1016/j.cej.2018.09.155

Zhu, Y., Yang, Y., Wang, X., Zhong, H., and Jin, F. (2019). Pd/C-catalyzed reduction of NaHCO3 into formate with 2-pyrrolidone under hydrothermal conditions. *Energy Sci. Eng.* 7, 881–889. doi:10.1002/ese3.317